Published in final edited form as:
Acad Radiol. 2011 August ; 18(8): 1014–1023. doi:10.1016/j.acra.2011.03.004.

Quantification of Regional Interstitial Lung Disease from CT-derived Fractional Tissue Volume: A Lung Tissue Research Consortium Study

Cuneyt Yilmaz, Ph.D.[a], **Snehal S. Watharkar, M.Sc.**[a], **Alberto Diaz de Leon, M.D.**[b], **Christine K. Garcia, M.D., Ph.D.**[a,b], **Nova C. Patel, M.D.**[c], **Kirk G. Jordan, M.D.**[c], and **Connie C.W. Hsia, M.D.**[a]

[a] Department of Internal Medicine, Division of Pulmonary and Critical Care Medicine, University of Texas Southwestern Medical Center, 5323 Harry Hines Blvd., Dallas, TX 75390-9034

[b] McDermott Center for Human Growth and Development, University of Texas Southwestern Medical Center, Dallas, TX

[c] Department of Radiology, University of Texas Southwestern Medical Center, Dallas, TX

Abstract

Rationale and Objectives—Evaluation of chest CT is usually qualitative or semi-quantitative, resulting in subjective descriptions often by different observers over time and imprecise determinations of disease severity within distorted lobes. There is a need for standardized imaging biomarkers to quantify regional disease, maximize diagnostic yield, and facilitate multi-center comparisons. We applied lobe-based voxelwise image analysis to derive regional air (Vair) and tissue (Vtissue) volumes and fractional tissue volume (FTV=tissue/[tissue+air] volume) as internally standardized parameter for assessing interstitial lung disease (ILD).

Materials and Methods—High-resolution CT was obtained at supine and prone end-inspiration and supine end-expiration in 29 patients with ILD and 20 normal subjects. Lobar Vair, Vtissue, and FTV were expressed along standard coordinate axes.

Results—In normal subjects from end-inspiration to end-expiration, total Vair declined 43%, FTV increased ~80% while Vtissue remained unchanged. With increasing ILD, Vair declined and Vtissue rose in all lobes; FTV increased with a peripheral-to-central progression inversely correlated to spirometry and lung diffusing capacity (R^2=0.57–0.75, prone end-inspiration). Inter- and intra-lobar coefficients of variation (CVs) of FTV increased 84–148% in mild-to-moderate ILD, indicating greater spatial heterogeneity, then normalized in severe ILD. Analysis of discontinuous images incurs <3% error compared to consecutive images.

Conclusions—These regional attenuation-based biomarkers could quantify heterogeneous parenchymal disease in distorted lobes, detect mild ILD involvement in all lobes and describe the pattern of disease progression. The next step would be to study a larger series, examine reproducibility and follow longitudinal changes in correlation with clinical and functional indices.

Address correspondence and requests for reprints to: Cuneyt Yilmaz, Ph.D., (214) 648-3426; fax (214) 648-8027, Cuneyt.Yilmaz@utsouthwestern.edu.

Keywords

*C*omputed tomography image analysis; lung air volume; lung tissue volume; lung tissue density; pulmonary fibrosis

Introduction

Pulmonologists increasingly rely upon volumetric computed tomography (CT) to diagnose and manage interstitial lung disease (ILD). Findings on CT have been reported to alter clinical decisions in 24 to 29% of cases, reduce the use of invasive diagnostic procedures by 16%, and improve agreement among clinicians on diagnostic probabilities (1). With widespread CT use comes the responsibility to ensure maximization of the diagnostic yield and minimization of the uncertainties associated with this technique in order to justify the small but real risk of harm due to cumulative radiation exposure (2), particularly in patients with chronic destructive lung disease who are routinely subjected to serial scans over many years. Up to now, clinical evaluation of chest CT remains mostly qualitative or semi-quantitative (1, 3, 4), resulting in unavoidable spatial, temporal, inter-observer and inter-scanner variability especially in multi-center clinical trials (5–7). The unique non-solid, elastic features of the lung renders the anatomy of the organ highly sensitive to volume change and asymmetric distortion due to non-uniform disease involvement; architectural distortion often makes it difficult to match the same anatomical regions on successive scans, especially if lung inflation changes. Furthermore, the large image dataset generated from each scan is routinely under-utilized. There is need for a comprehensive, objective and quantitative approach to fully exploit the information content and diagnostic potential of this powerful tool. Quantitative lobe-based approach has not been widely adopted partly because of the perceived effort required and partly because of a lack of examples showing how specific imaging biomarkers could be standardized in application to clinical pathology.

To address some of these issues, we developed a PC-based semi-automated algorithm to map and analyze lung attenuation within each lobe in a voxelwise fashion. By referencing the voxel attenuation with respect to internal calibrators for intra-thoracic air and tissue in each subject, standardized air and tissue volumes and “fractional tissue volume” (FTV) were derived as regional anatomical markers that could be mapped with respect to reference coordinate axes of each lobe and compared within and among lobes. The novel approach has been shown in animals to accurately characterize nonuniform regional structural lung growth during postnatal maturation and postpneumonectomy compensation (8–10) but has not been applied to clinical disease. We employed this technique to analyze high-resolution chest CT obtained in patients with ILD to describe lobar disease severity and test the hypothesis that the magnitude, spatial distribution and heterogeneity of CT-derived indices objectively reflect abnormalities in spirometry and lung diffusing capacity (DL_{CO}).

Materials and methods

Subjects

The Lung Tissue Research Consortium (LTRC, http://www.nhlbi.nih.gov/resources/ltrc.htm), sponsored by the National Heart, Lung and Blood Institute, provided from its multi-center databank non-contrasted high resolution CT (HRCT) studies obtained at supine end-inspiration, supine end-expiration, and prone end-inspiration from 29 patients with ILD, categorized by FVC (% predicted): mild (>=80%), moderate: (50–80%), severe (30–50%) and more severe (<30%). All patients had biopsy-confirmed pathological diagnosis of usual interstitial pneumonitis (UIP, n=23) or uncharacterized fibrosis (n=6). Clinical symptoms and pulmonary function tests were also

provided. All patients provided written informed consent to the LTRC. For control data, we obtained similar set of high-resolution CT images and pulmonary function tests from 20 healthy volunteers who served as control subjects in a separate study approved by the Institutional Review Board of the University of Texas Southwestern Medical Center (UT Southwestern). Written informed consent was obtained from all subjects. Spirometry and DL_{CO} were measured by a breath hold method in keeping with recommendations of the American Thoracic Society (11, 12).

HRCT

For ILD, all LTRC participating centers used Gammex 464 CT phantom (Gammex, Middleton, WI) for scanner calibration. Three helically acquired datasets were obtained by a multi-detector scanner (at least 8 detectors, 140 kVp, 324 mA) optimized to allow single breath acquisition in <15 s. Images were rendered at consecutive 0.625 mm intervals from apex to costophrenic angle (~400 images per patient). For normal subjects studied at UT Southwestern, Catphan500 (The Phantom Laboratory, Salem, NY) was used to calibrate the scanner (GE Light speed 16, Milwaukee, WI). Discontinuous 1.25 mm thick images were obtained at 10 mm intervals from apex to base (~40 images per subject). In all studies, scout images were obtained to ensure that the field of scan included the entire lung, followed by imaging at supine end-inspiration, supine end-expiration, and prone end-inspiration.

Image analysis

DICOM images were reconstructed using standard reconstruction algorithm and analyzed using a semi-automated algorithm developed in our laboratory (Visual C++ 6.0 with OpenGL library) (8–10). Lung area on each image was outlined by density thresholding, excluding the trachea and next 3 generations of airways and blood vessels. Computer-generated pleural boundaries were manually verified and adjusted as necessary. Key points along inter-lobar fissures were manually identified every 10^{th} image and fitted with cubic splines. On the intervening images the algorithm interpolated the fissures and the interpolation was verified visually. Inter-lobar fissures were readily identifiable in most patients. In two patients with “more severe” ILD it was difficult to discern the fissures on some images and these were interpolated. Each lobe was reconstructed in 3D and analyzed separately. The lingula was included as part of the left upper lobe (LUL). Lung volume was calculated as Σ(area × slice thickness).

Attenuation-derived indices

CT attenuations of extra-thoracic air and water were set at −1,000 and 0 HU, respectively. Attenuation of intra-thoracic air was measured as the average of 3 points at the center of the tracheal column 5 mm above carina (range −1090 to −1100 HU). Assuming that average CT number (CT_n) of air-free lung tissue (including blood) equals that of muscle, we averaged the attenuation at the center of infraspinatus, supraspinatus and pectoralis muscles at the level just above carina (control subjects 58±3 HU, ILD 50±15 HU, mean ± SD). The average CT numbers of intratracheal air (air CTn) and air-free tissue (muscle CTn) were used in conjunction with that of the lobe (lobar CTn) to partition the total lobar volume into air and tissue volumes:

$$Lobar\ tissue\ volume = \frac{Lobar\ CT_n - air\ CT_n}{muscle\ CT_n - air\ CT_n} \times total\ lobar\ volume. \quad \text{Eq. 1}$$

$$Lobar\ air\ volume = total\ lobar\ volume - lobar\ tissue\ volume \quad \text{Eq. 2}$$

$$Fractional\ tissue\ volume = \frac{lobar\ tissue\ volume}{total\ lobar\ volume} \quad \text{Eq. 3}$$

In addition, we measured the attenuation of the right lobe of liver as an alternative internal calibrator of tissue attenuation and compared the results with that obtained using muscle attenuation.

Images with and without gaps

Initially, every image in ILD patients was analyzed exhaustively (~400 images 0.625 mm apart). In 4 patients we repeated the analysis using every 10^{th} image (~40 images 6.25 mm apart). Using images with gaps resulted in negligible error (range 0.01% to 3%) in derived indices: air volume, tissue volume and FTV compared to that using all consecutive images. Therefore, subsequent analysis was performed using every 10^{th} image in the dataset.

Air volume, tissue volume and FTV derived from each voxel were plotted along 3 coordinate axes: x (medial-to-lateral), y (posterior-to-anterior) and z (cephalad-to-caudal). Each axis was classified into bins: 0–10%, 10–30%, 30–50%, 50–70%, 70–90% and 90–100%, of total span and analyzed with respect to average positions of the bin along a given axis i.e., 5, 20, 40, 60, 80 and 95%. Coefficients of variation (CV=SD/mean) of FTV within and among lobes were calculated to assess heterogeneity.

Statistical Analysis

Data were expressed as mean ± SD and compared with respects to posture, lung inflation and subject groups using factorial ANOVA. Kurtosis and skewness of the FTV distribution was compared to known critical values. Intra- and inter-lobar comparisons were performed by repeated measures ANOVA. Post-hoc test was performed by Fishers protected least significant difference. $P \leq 0.05$ was considered significant.

Results

Demographic and lung function data are summarized in separate categories of progressive lung restriction (Table 1). The mean attenuation values, the derived FTV and its histogram are shown in Table 2. Muscle attenuation was significantly lower and more variable in ILD (45±18 HU, mean ± SD) than control (58±3 HU) subjects; the difference causes up to 3.4% deviation in tissue volume estimates but did not alter the conclusions of statistical analysis. The attenuation of liver is not different between ILD and normal subjects. Using liver instead of muscle attenuation in the calculation caused less than 4.4% change in tissue volume and FTV and less than 2% change in air volume, and did not alter the conclusions of statistical analysis. In both ILD and control groups, kurtosis and skewness of the FTV histogram are within the range of a normal distribution.

Figure 1 shows examples of axial images (**top**), the corresponding axial color FTV maps (**middle**), and 3D surface FTV maps (**bottom**) for one representative subject in each category. Early ILD predominantly involved the lower lobes and the periphery of each lobe. With increasing ILD severity there was a progressive increase in patchy regions of high FTV in all lobes. Mean lobar air and tissue volumes and average FTV are quantified in Figure 2; corresponding values for both lungs are shown in Figure 3. In normal subjects from end-inspiration to end-expiration, total air volume decreased ~43% and FTV increased ~80% while total tissue volume remained constant; the constancy of tissue volume validates the use of internal control parameters in this analysis. In mild ILD there was a modest increase (~35%) in overall lung tissue volume. With increasing ILD severity, lobar as well

as whole lung air volume decreased while the corresponding tissue volume increased by up to 70% except in the 2 patients with “more severe” ILD who exhibited marked contraction of air volume without further increase in tissue volume. Supine FTV was systematically higher in the left and right lower lobes (LLL and RLL, respectively) than the upper lobes (LUL and RUL, respectively) or right middle lobe (RML); difference among lobes were exaggerated in ILD but disappeared at prone end-inspiration (Figure 2). In mild ILD, mean lobar FTV did not differ significantly from normal. In moderate to severe ILD, FTV progressively rose in all lobes and more at supine end-expiration than at supine or prone end-inspiration. In “more severe” ILD, FTV either declined or showed no further change compared to severe ILD.

Intra-lobar gradients of regional FTV are shown for all lobes at prone end-inspiration in Figure 4. In normal lungs intra-lobar FTV was relatively uniform (averaging 0.120, 0.109 and 0.188 at prone-inspiration, supine-inspiration and supine-expiration, respectively). In mild ILD, FTV increased modestly but significantly in peripheral regions and along each coordinate axis of all lobes, especially in lower lobes. With increasing ILD severity, intra-lobar FTV became elevated in all regions (up to 5-fold above normal) while the central-to-peripheral FTV gradient in each lobe was preserved or accentuated (by up to 135%) in advanced ILD. Thus, statistically significant inter- and intra-lobar gradients FTV, reflecting the heterogeneity as well as severity of ILD, were detected in all lobes. The consistent pattern of lobe-by-lobe results with respect to posture, respiratory phase and ILD severity also strengthens the validity of our analysis. In all lobes, FTV significantly correlated with FEV_1, FVC and DL_{CO} in all scans regardless of posture or lung inflation (shown for right lower lobe in Figure 5).

The coefficient of variation of FTV among lobes (inter-lobar CV) increased 84% with moderate ILD and then normalized with more advanced ILD (Figure 6, left panel). The CV of FTV within each lobe (intra-lobar CV) increased 148% above normal in mild ILD, consistent with the development of patchy early anatomical abnormalities. With increasing ILD severity, intra-lobar CV of FTV declined towards normal values, consistent with progression towards diffuse anatomical involvement (Figure 6, right panel). These changes were most pronounced at prone end-inspiration.

Discussion

Summary of results

This study tests CT-derived regional air and tissue volumes and FTV as non-invasive markers of ILD distribution and severity. These parameters tracked the expected changes with lung inflation and increasing ILD severity. In addition, we mapped regional FTV in each lobe along standardized coordinate axes across the spectrum of ILD severity and correlated regional FTV magnitude and heterogeneity with lung function. The main findings are: a) Regional FTV increased with increasing ILD severity in a peripheral-to-central progression within each lobe, b) lobar mean FTV correlated inversely with FEV_1, FVC and DL_{CO} at supine and prone end-inspiration and supine end-expiration, c) FTV heterogeneity among and within lobes became significantly elevated in mild-to-moderate ILD, then declined towards normal values in more advanced ILD. Results demonstrate the feasibility of this technique in mapping irregular parenchymal pathology in distorted lobes, and the functional relevance of these imaging biomarkers. Furthermore, images may be obtained or analyzed at nonconsecutive intervals (6.25 to 10 mm apart) without loss of quantitative information, making this analysis applicable to clinical imaging protocols.

Quantitative image analysis

Various studies have compared computer-based segmentation and quantification of lung attenuation with visual scoring of CT images in diffuse lung disease (13–15), demonstrating that quantitative analysis yields more robust and reproducible results than qualitative evaluation (13, 16). By applying automated thresholding algorithms, attenuation threshold values have been used to calculate global and regional mean lung density (17) and show that mean lung density is elevated above normal or that the histogram of lung attenuation shifts towards higher values in idiopathic pulmonary fibrosis (13, 18–20). CT attenuation has been used in idiopathic pulmonary fibrosis to calculate the proportion of whole lung tissue and air, and this value was used to correct histological measurements made on lung biopsy specimens to the level of inflation during the CT scan (21). In ILD quantitative CT indexes calculated for the entire lung correlated with physiological impairment (13, 22). Automated analysis for comparing paired CT studies at baseline and follow-up has also been described (23). However, no attempt was made to systematically map and quantify the attenuation gradients or their heterogeneity within and among lobes. In addition, multi-center studies of computer-assisted attenuation analysis have raised persistent questions of inter-scan variability due to different CT platforms and models, beam hardening artifacts and differences in lung volume during scanning (24, 25). A standardized biomarker calibrated with respect to internal references in each subject would control for the possible sources of variability thereby allowing more accurate data comparisons among lung regions, subjects as well as study centers.

Significance

This study made several contributions: 1) Mapping along standardized 3D axes of each lobe allows comparisons of the corresponding regions within their natural anatomical compartments at different inflation states and postures. As long as the inter-lobar fissures are identifiable, the same lobes could be followed even in the presence of architectural distortion, displacement or collapse. 2) Regional air and tissue volumes and FTV could serve as quantitative markers to follow irregular changes in the course of ILD, e.g., comparing the improvement of infiltrates in one lobe with deterioration in another. 3) One advantage of comparing FTV instead of attenuation is that FTV is calibrated with respect to internal references, i.e., that of intra-thoracic air and air-free tissue in each subject, which eliminates much of the variability from multiple centers and different scanner models, allowing data standardization for objective comparison. 4) Inter-regional variability of FTV indexed by its CV within and among lobes could serve as markers of spatial disease heterogeneity. In at-risk patients, e.g., occupational exposure or kindred of familial idiopathic pulmonary fibrosis, an increase in the CV of FTV may herald early onset of clinical ILD. In established ILD, a decline in the CV of FTV may signal disease progression. 5) We showed that ILD progresses in a similar topological pattern in all lobes such that lobe-based FTV indexes global pulmonary dysfunction. These findings established the utility and clinical relevance of lobe-based image analysis in the assessment of heterogeneous lung pathology.

Limitations of the study

The LTRC datasets were collected from several participating centers using different CT scanners but standardized imaging protocols. The number of patients in the “more severe” ILD group was small (n=2) and DL_{CO} was not available. End-inspiration and end-expiration were not verified by respiratory pressure measurements, which could have led to variability in FTV with respect to respiratory phase. The automated attenuation thresholding for isolating the area occupied by lung on each image may be subject to errors if significant pleural fibrosis is present. In such cases, the computer-detected pleural boundaries are manually verified. CT-derived tissue volume includes the volume of blood vessels,

microvascular blood, and extra-vascular tissue; these could not be differentiated on non-contrasted scans. The attenuation-based FTV cannot quantify textural or patterning abnormalities such as ground glass opacity, reticular infiltrates and honeycombing. Texture-based methods such as adaptive multiple feature and fractal analysis that are currently being developed may help to identify and quantify these abnormal patterns (26–29) to complement the assessment of FTV. The standard reconstruction algorithm was used in all scans to minimize variability in mean lung attenuation and its frequency distribution histogram caused by different reconstruction algorithms (30). Disuse, atrophy, fatty infiltration, inflammation or steroid use can alter skeletal muscle attenuation (31) resulting in modest variability on a subject's air volume, tissue volume and FTV. One alternative internal reference is to use the attenuation of liver, which could reduce data variability in ILD subjects as long as there is no significant liver disease. In addition to this cross-sectional study, longitudinal follow-up will be needed to verify the reproducibility of internal references and the derived CT biomarkers. Finally, most patients had UIP; further studies will determine how well this analysis applies to other patterns of ILD.

Conclusions

We presented a quantitative method to determine the severity of regional fibrosing ILD for comparison within and among lobes. This method describes the normal 3D spatial gradients of FTV as well as the exaggerated gradients that develop in a peripheral-to-central progression across all lobes with increasing ILD severity. There are significant correlations between the magnitude and heterogeneity of regional FTV and global lung function. This lobe-based image analysis increases voxel information yield and provides objective and functionally relevant anatomical markers of ILD even in the face of irregular lobar distortion. The next step would be to study a larger patient sample, examine reproducibility and longitudinally follow disease severity in correlation with lung function. An analogous approach could be used in other parenchymal diseases such as emphysema. One immediate application of this approach is in standardized analysis of imaging data from multi-center clinical trials, which could improve subject stratification, objective monitoring and evaluation of regional anatomical response to treatment. With additional automation of the analytical steps, this approach may ultimately assist pulmonologists and radiologists in clinical decision-making. Improving the diagnostic yield from CT study could benefit patients and physicians alike by reducing the need for repeated scans or more invasive diagnostic tests.

Acknowledgments

Supported by: National Heart, Lung, and Blood Institute grants R03 HL097010 (CY), R01 HL093096 (CKG), a pilot award (to CCH) by the North and Central Texas Clinical and Translational Science Initiative UL1 RR024982, and the American Heart Association (CKG). The Lung Tissue Research Consortium was supported by the National Center for Research Resources UL1 RR024150.

References

1. Aziz ZA, Wells AU, Bateman ED, Copley SJ, Desai SR, Grutters JC, Milne DG, Phillips GD, Smallwood D, Wiggins J, et al. Interstitial lung disease: effects of thin-section CT on clinical decision making. Radiology. 2006; 238:725–733. [PubMed: 16344334]
2. Smith-Bindman R. Is computed tomography safe? N Engl J Med. 2010; 363:1–4. [PubMed: 20573919]
3. Goldin JG, Lynch DA, Strollo DC, Suh RD, Schraufnagel DE, Clements PJ, Elashoff RM, Furst DE, Vasunilashorn S, McNitt-Gray MF, et al. High-resolution CT scan findings in patients with symptomatic scleroderma-related interstitial lung disease. Chest. 2008; 134:358–367. [PubMed: 18641099]

4. Zompatori M, Bna C, Poletti V, Spaggiari E, Ormitti F, Calabro E, Tognini G, Sverzellati N. Diagnostic imaging of diffuse infiltrative disease of the lung. Respiration. 2004; 71:4–19. [PubMed: 14872104]
5. Li F, Kumazawa S, Shiraishi J, Li Q, Engelmann R, Caligiuri P, MacMahon H, Doi K. Subjective similarity of patterns of diffuse interstitial lung disease on thin-section CT: an observer performance study. Acad Radiol. 2009; 16:477–485. [PubMed: 19268860]
6. Armato SG 3rd, McNitt-Gray MF, Reeves AP, Meyer CR, McLennan G, Aberle DR, Kazerooni EA, MacMahon H, van Beek EJ, Yankelevitz D, et al. The Lung Image Database Consortium (LIDC): an evaluation of radiologist variability in the identification of lung nodules on CT scans. Acad Radiol. 2007; 14:1409–1421. [PubMed: 17964464]
7. Van de Steene J, Linthout N, de Mey J, Vinh-Hung V, Claassens C, Noppen M, Bel A, Storme G. Definition of gross tumor volume in lung cancer: inter-observer variability. Radiother Oncol. 2002; 62:37–49. [PubMed: 11830311]
8. Ravikumar P, Yilmaz C, Dane DM, Johnson RL Jr, Estrera AS, Hsia CC. Regional lung growth following pneumonectomy assessed by computed tomography. J Appl Physiol. 2004; 97:1567–1574. discussion 1549. [PubMed: 15208290]
9. Ravikumar P, Yilmaz C, Dane DM, Johnson RL Jr, Estrera AS, Hsia CC. Developmental signals do not further accentuate nonuniform postpneumonectomy compensatory lung growth. J Appl Physiol. 2007; 102:1170–1177. [PubMed: 17138837]
10. Yilmaz C, Ravikumar P, Dane DM, Bellotto DJ, Johnson RL Jr, Hsia CC. Noninvasive quantification of heterogeneous lung growth following extensive lung resection by high-resolution computed tomography. J Appl Physiol. 2009; 107:1569–1578. [PubMed: 19729592]
11. American Thoracic Society. Standardization of Spirometry, 1994 Update. Am J Respir Crit Care Med. 1995; 152:1107–1136. [PubMed: 7663792]
12. American Thoracic Society. Single-breath carbon monoxide diffusing capacity (transfer factor). Recommendations for a standard technique--1995 update. Am J Respir Crit Care Med. 1995; 152:2185–2198. [PubMed: 8520796]
13. Camiciottoli G, Orlandi I, Bartolucci M, Meoni E, Nacci F, Diciotti S, Barcaroli C, Conforti ML, Pistolesi M, Matucci-Cerinic M, et al. Lung CT densitometry in systemic sclerosis: correlation with lung function, exercise testing, and quality of life. Chest. 2007; 131:672–681. [PubMed: 17356079]
14. Revel MP, Faivre JB, Remy-Jardin M, Deken V, Duhamel A, Marquette CH, Tacelli N, Bakai AM, Remy J. Automated lobar quantification of emphysema in patients with severe COPD. Eur Radiol. 2008; 18:2723–2730. [PubMed: 18604539]
15. Zavaletta VA, Bartholmai BJ, Robb RA. High resolution multidetector CT-aided tissue analysis and quantification of lung fibrosis. Acad Radiol. 2007; 14:772–787. [PubMed: 17574128]
16. Lynch DA. Quantitative CT of fibrotic interstitial lung disease. Chest. 2007; 131:643–644. [PubMed: 17356073]
17. Kalender WA, Fichte H, Bautz W, Skalej M. Semiautomatic evaluation procedures for quantitative CT of the lung. J Comput Assist Tomogr. 1991; 15:248–255. [PubMed: 2002103]
18. Hoffman EA, Reinhardt JM, Sonka M, Simon BA, Guo J, Saba O, Chon D, Samrah S, Shikata H, Tschirren J, et al. Characterization of the interstitial lung diseases via density-based and texture-based analysis of computed tomography images of lung structure and function. Acad Radiol. 2003; 10:1104–1118. [PubMed: 14587629]
19. Lamers RJ, Kemerink GJ, Drent M, van Engelshoven JM. Reproducibility of spirometrically controlled CT lung densitometry in a clinical setting. Eur Respir J. 1998; 11:942–945. [PubMed: 9623701]
20. Hartley PG, Galvin JR, Hunninghake GW, Merchant JA, Yagla SJ, Speakman SB, Schwartz DA. High-resolution CT-derived measures of lung density are valid indexes of interstitial lung disease. J Appl Physiol. 1994; 76:271–277. [PubMed: 8175517]
21. Coxson HO, Hogg JC, Mayo JR, Behzad H, Whittall KP, Schwartz DA, Hartley PG, Galvin JR, Wilson JS, Hunninghake GW. Quantification of idiopathic pulmonary fibrosis using computed tomography and histology. Am J Respir Crit Care Med. 1997; 155:1649–1656. [PubMed: 9154871]

22. Best AC, Lynch AM, Bozic CM, Miller D, Grunwald GK, Lynch DA. Quantitative CT indexes in idiopathic pulmonary fibrosis: relationship with physiologic impairment. Radiology. 2003; 228:407–414. [PubMed: 12802000]

23. Arzhaeva Y, Prokop M, Murphy K, van Rikxoort EM, de Jong PA, Gietema HA, Viergever MA, van Ginneken B. Automated estimation of progression of interstitial lung disease in CT images. Med Phys. 2010; 37:63–73. [PubMed: 20175467]

24. Covino SW, Mitnick RJ, Shprintzen RJ, Cisneros GJ. The accuracy of measurements of three-dimensional computed tomography reconstructions. J Oral Maxillofac Surg. 1996; 54:982–990. discussion 990-981. [PubMed: 8765388]

25. Bakker ME, Stolk J, Putter H, Shaker SB, Parr DG, Piitulainen E, Russi EW, Dirksen A, Stockley RA, Reiber JH, et al. Variability in densitometric assessment of pulmonary emphysema with computed tomography. Invest Radiol. 2005; 40:777–783. [PubMed: 16304481]

26. Xu Y, Sonka M, McLennan G, Guo J, Hoffman EA. MDCT-based 3-D texture classification of emphysema and early smoking related lung pathologies. IEEE Trans Med Imaging. 2006; 25:464–475. [PubMed: 16608061]

27. Xu Y, van Beek EJ, Hwanjo Y, Guo J, McLennan G, Hoffman EA. Computer-aided classification of interstitial lung diseases via MDCT: 3D adaptive multiple feature method (3D AMFM). Acad Radiol. 2006; 13:969–978. [PubMed: 16843849]

28. Uppaluri R, Hoffman EA, Sonka M, Hunninghake GW, McLennan G. Interstitial lung disease: A quantitative study using the adaptive multiple feature method. Am J Respir Crit Care Med. 1999; 159:519–525. [PubMed: 9927367]

29. Wang J, Li F, Li Q. Automated segmentation of lungs with severe interstitial lung disease in CT. Med Phys. 2009; 36:4592–4599. [PubMed: 19928090]

30. Koyama H, Ohno Y, Yamazaki Y, Nogami M, Kusaka A, Murase K, Sugimura K. Quantitatively assessed CT imaging measures of pulmonary interstitial pneumonia: effects of reconstruction algorithms on histogram parameters. Eur J Radiol. 2010; 74:142–146. [PubMed: 19324507]

31. Kelley, DE.; Storlien, L. Skeletal muscle and obesity. In: Bray, GA.; Bouchard, C., editors. Handbook of obesity, Part II, Etiology. Vol. Chapter 29. New York: Marcel Dekker; 2004.

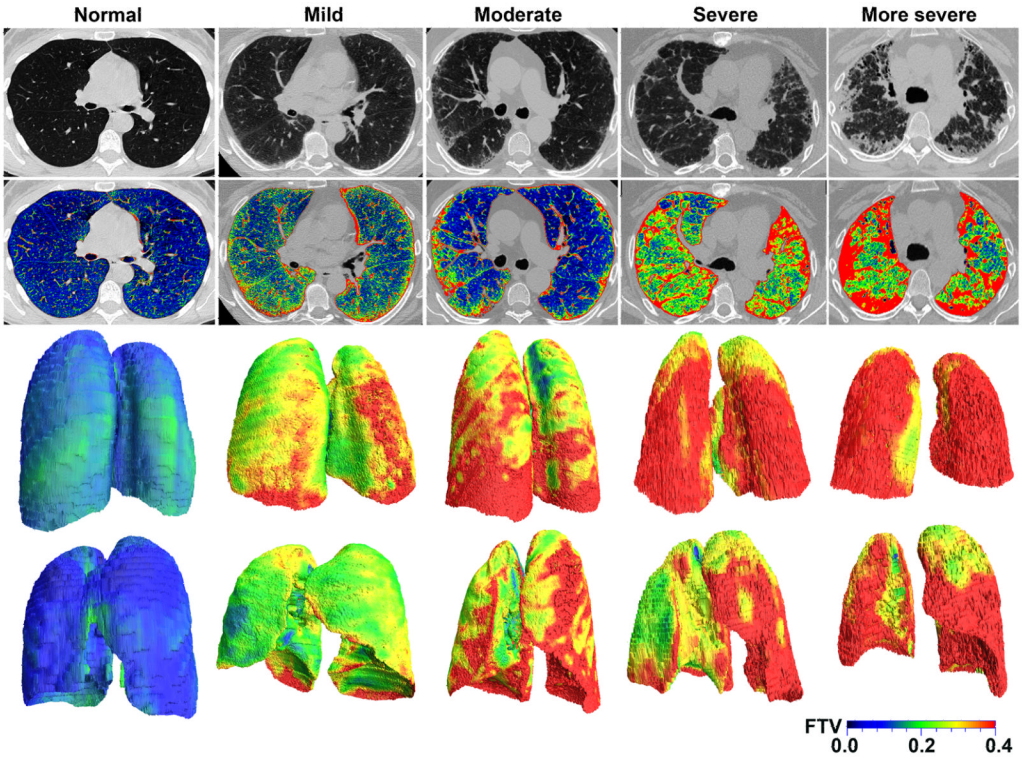

Figure 1.
Representative axial HRCT images (top panels), color maps of FTV (middle panels), and the three-dimensional surface color maps of FTV (bottom panels in two orientations) from one normal subject and one subject each with mild, moderate, severe and more severe ILD (groups **I** through **V** respectively).

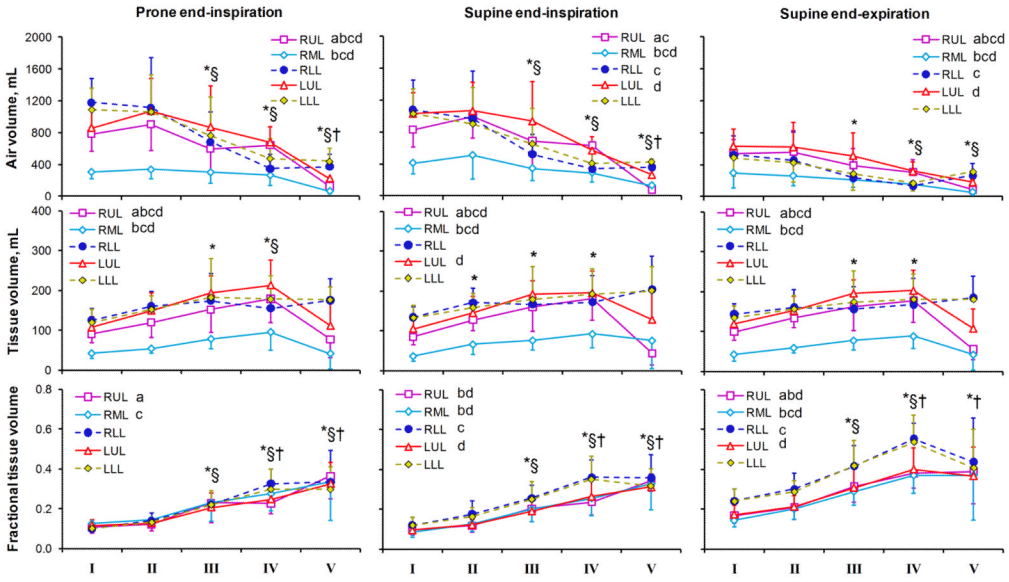

Figure 2.

Lobar air and tissue volumes and FTV are shown at prone end-inspiration, supine end-inspiration and supine end-expiration for each ILD group: normal, mild, moderate, severe and more severe (groups **I** through **V**, respectively). Mean ± SD. P<0.05 * vs. **I** (normal); **§** vs. **II** (mild); **†** vs. **III** (moderate); **a** vs. RML; **b** vs. RLL; **c** vs. LUL; and **d** vs. LLL, by repeated measures ANOVA.

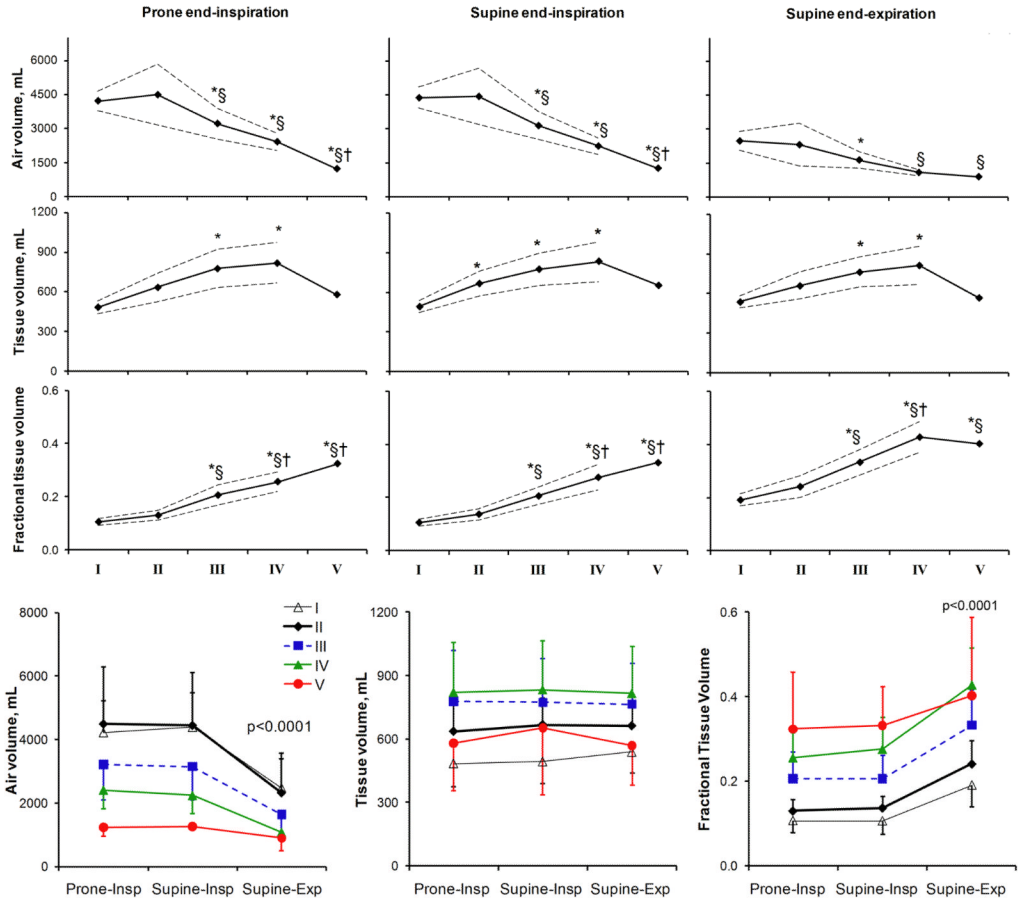

Figure 3.

A) Total air volume, total tissue volume, and average whole lung FTV are shown with respect to ILD severity: normal, mild, moderate, severe and more severe (groups **I** through **V**, respectively). Dashed lines denote upper and lower 95% confidence intervals (omitted for Group V due to the small number of subjects). * $p<0.05$ vs. **I** (normal); **§** vs. **II** (mild)**, †** vs. **III** (moderate) by repeated measures ANOVA. B) The same data are shown with respect to posture and respiratory phase in each group. Air volume was significantly lower and FTV higher at supine-expiration than prone-inspiration or supine-inspiration (mean ± SD, $p<0.0001$ by repeated measures ANOVA). Total tissue volume did not change significantly with posture or respiratory phase.

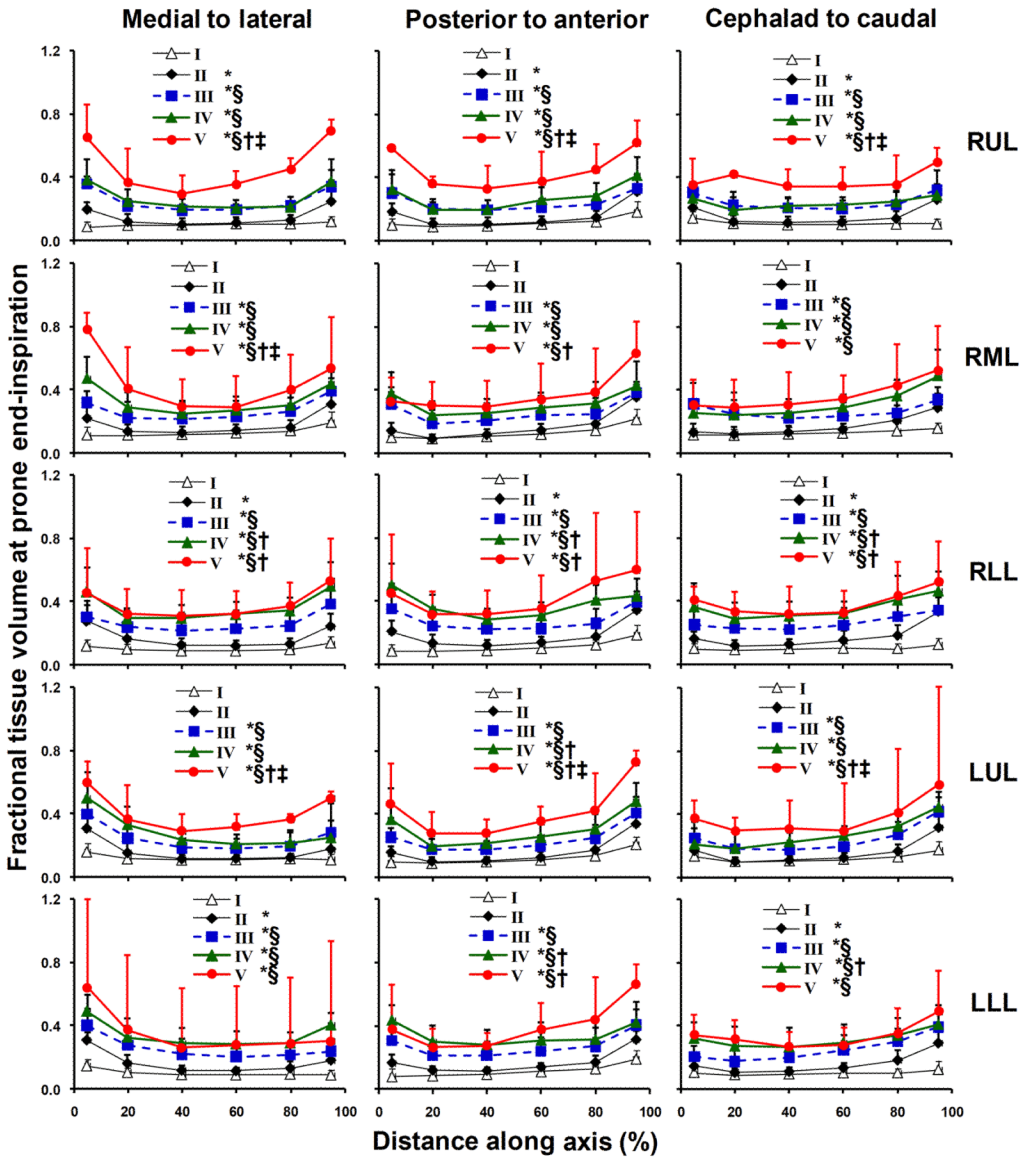

Figure 4.

Intra-lobar distribution of FTV at prone end-inspiration is shown with respect to the position (% of the total span) along a given axis in each lobe. Mean ± SD. * $p<0.05$ vs. **I** (normal); § vs. **II** (mild), † vs. **III** (moderate); ‡ vs. **IV** (severe) by repeated measures ANOVA.

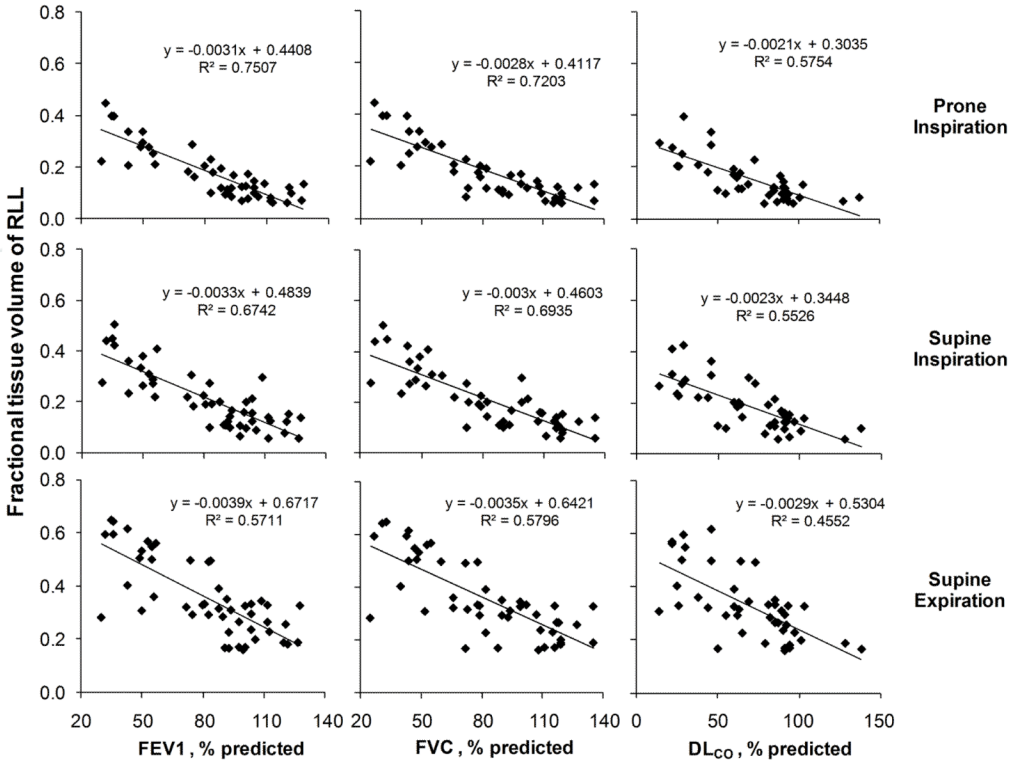

Figure 5.

Mean lobar FTV correlated inversely with FEV_1, FVC and DL_{CO} (% predicted) at prone end-inspiration, supine end-inspiration, and supine end-expiration (shown for the right lower lobe only, all $p<0.001$).

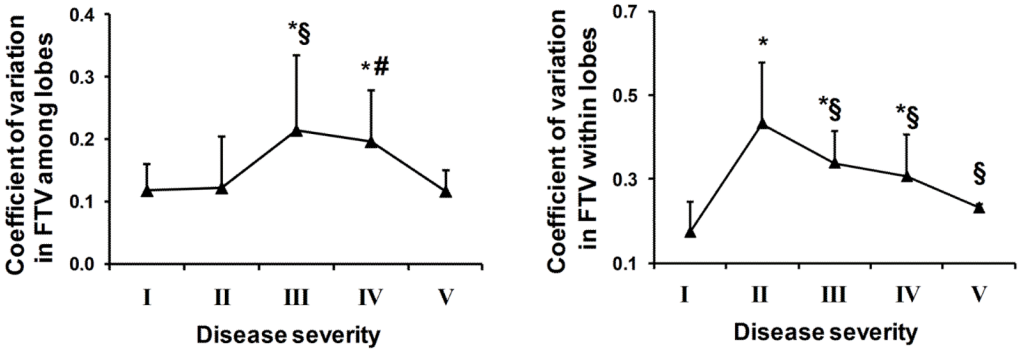

Figure 6.

Coefficients of variation (CV's) of FTV among lobes (*left panel*) and within lobes (*right panel*) at prone end-inspiration are shown with respect to ILD severity groups. Mean ± SD. * $p<0.05$ vs. **I** (normal); **§** $p<0.05$ and # $p=0.06$ vs. **II** (mild) by factorial ANOVA.

Table 1

Demographic data and lung function

Group	**I**	**II**	**III**	**IV**	**V**
ILD severity	**Normal**	**Mild**	**Moderate**	**Severe**	**More Severe**
Number of subjects	20	7	11	9	2
Male/female	11/9	3/4	7/4	6/3	0/2
Age, yrs	51±12	64±9	57±15	55±6	40±19
Height, cm	171±12	168± 9	170±9	169±10	167±3
Weight, kg	79±23	82±12	87±16	79±17	65±22
BMI, $kg \cdot m^{-2}$	28.8±11.7	42.6±3.6	43.4±4.1	41.7±4.1	37.5±8.0
Hemoglobin, $g \cdot dL^{-1}$	13.7 ± 1.4	14.4±1.4	14.7±1.2	13.2±1.8	13.0
FEV_1, L	3.33±0.90	2.64±0.50	2.15±0.49	1.44±0.40	1.00±0.14
FEV_1, % predicted	105±14	96±7	71±14	45±8	31±1
FVC, L	4.28±1.10	3.46±0.82	2.69±0.67	1.77±0.44	1.05±0.07
FVC, % predicted	111±15	90±13	67±10	42±6	26±1
FEV_1/FVC, % predicted	95±5	107±13	106±11	106±12	119±1
DL_{CO}, $mL \cdot [min \cdot mmHg]^{-1}$	23.3±5.9	15.4±5.3	10.2±4.7	7.5±2.8	-
DL_{CO}, % predicted	88±17	77±32	45±23	32±8	-

Mean ± SD.

Table 2

Attenuation values and Histogram of FTV

	Normal (n=20)	ILD (n=29)
Attenuation (HU)		
Tracheal air	−969 ± 9	−971 ± 14
Thoracic muscle	58 ± 3	45 ± 18 *
Liver	64 ± 9	59 ± 9
Histogram of FTV (using muscle attenuation)		
Prone End-Inspiration		
Mean lung FTV	0.106 ± 0.029	0.210 ± 0.082 *
Kurtosis	−0.558	0.041
Skewness	0.368	0.814
Supine End-Inspiration		
Mean lung FTV	0.106 ± 0.030	0.220 ± 0.083 *
Kurtosis	0.341	−0.101
Skewness	0.711	0.682
Supine End-Inspiration		
Mean lung FTV	0.191 ± 0.051	0.345 ± 0.108 *
Kurtosis	−0.172	−0.450
Skewness	0.703	0.526
Critical values (p<0.05 2-sided)		
Kurtosis (range of normality)	−1.27 to, 2.56	−1.08 to 2.12
Skewness	1.03	0.847

Mean ± SD.

* p<0.05 vs. Normal.